An Examination of the Applicability of Computed Tomography for the Measurement of Component Concentrations in Fire-Generated Plumes

ROBERT T. BAUM, KEVIN B. MCGRATTAN, and MARC R. NYDEN*
Building and Fire Research Laboratory, National Institute of Standards and Technology, Gaithersburg, MD 20899, USA

The purpose of this investigation is to examine the feasibility of using computed tomography to evaluate the predictive capabilities of fire models. In this pursuit, we have analyzed data from both laboratory- and computer-generated plumes in order to determine the number of line-of-sight measurements, the detector topology, and the temporal resolution needed to obtain accurate reconstructions of component concentrations in fire atmospheres. © 1998 by The Combustion Institute

INTRODUCTION

One of the major goals of fire research is to develop the capability to make realistic assessments of fire impact and risk. The development of the measurement technology needed to perform rigorous evaluations of the predictive capabilities of fire models is an essential step toward the attainment of this goal. At a minimum, this will require the ability to make time-dependent measurements of the distribution of both smoke and gases in room-scale enclosures ($\sim$30 m^3 in volume) with a spatial resolution of a few centimeters and a temporal resolution of about 100 Hz. This measurement density is much too high to achieve using conventional point sampling techniques such as the thermocouples and gas sampling probes [1, 2]. We propose to address this technical deficiency by applying computed tomography [3–12], which is based on line-of-sight rather than point measurements, in making accurate, time-resolved, three-dimensional measurements of component concentrations in fire environments.

Computed tomography is already a mature technology with many routine applications in medical imaging [12] and nondestructive evaluation [3]. Typical commercial tomographic systems utilize a source of monochromatic x-rays in configurations that produce images with high spatial resolution and low temporal resolution over a well-defined sample volume in a controlled environment. While these systems have been very successful in medical and industrial settings, they are not suitable for application to the problem of interest that requires the capability to image large, time-dependent flow fields with quantitative accuracy. The further development of this measurement technique, to the point where it can provide accurate descriptions of the transport of smoke and gases in turbulent plumes, presents a significant challenge because of the dynamic nature of the measurements, the physical dimensions of the volume, and the adverse conditions of the measurement space. The wavelength of the radiation (i.e., infrared rather than x-ray) is also an issue because of the limitations of available infrared detectors, the potential for beam steering due to varying refractive indices, and the background emissions from the plume which are primarily in the mid-infrared region. Furthermore, broadband infrared detectors, which allow for a large range of compounds to be quantified and identified, are much more expensive (on a per element basis) and less responsive than the x-ray detectors that are used in conventional CT scanning devices. On the other hand, fire-generated plumes often exhibit an underlying axisymmetry that implies that the angular concentration gradients within the plume are small. This effect, when coupled with the reduction in the radial component of the concentration gradients that results from dilution of the plume by air entrained from the surrounding atmosphere, makes it likely that accurate reconstructions can be obtained from considerably less line-of-sight data than is routinely used in medical or indus-

*Corresponding author.

0010-2180/98/$19.00
PII: S0010-2180(97)00219-8

trial applications where high resolution images are needed to resolve small defects in irregular objects. The expectation is that any flexibility in the density of line-of-sight measurements needed to characterize the spatial dependence of the component concentrations can be exploited to provide the increases in temporal resolution, quantitative accuracy, and the physical dimensions of the measurement space that are needed to capture the full turbulent structure of fire-generated plumes.

Previous research conducted in this laboratory has demonstrated the applicability of computed tomography in the reconstruction of probability density functions (pdfs) that describe local property fields in turbulent jet diffusion flames [13, 14]. Tomographic reconstruction techniques also have been used to study the effects of reduced gravity on the spatial distribution of soot in droplet combustion [15] and laminar acetylene jet diffusion flames [16]. The purpose of this investigation is to assess the feasibility of extending this capability to obtain accurate, time resolved, three-dimensional measurements of component concentrations in the vicinity of large fires. In this pursuit, we have analyzed data from both laboratory- and computer-generated plumes in order to determine the reconstruction error as a function of the number of line-of-sight measurements. The rate of convergence of the reconstructions with respect to the angular resolution of the measurements is of particular interest, since the number of view angles that can be accommodated is a critical factor in the design of a tomographic spectrometer.

BACKGROUND

Spectroscopic measurements of component concentrations are made on the basis of Beer's law, which is summarized in Eq. (1),

$$A_\nu(r,\theta) \equiv -\log\left(\frac{I_\nu}{I_{0\nu}}\right) = \alpha_\nu l C_i. \tag{1}$$

In this equation, A_ν is the absorbance at the frequency ν (expressed in wavenumber units), that is defined as the (base 10) logarithm of the ratio of the intensities of the incident ($I_{0\nu}$) to the transmitted (I_ν) radiation, α_ν is the absorption coefficient, 1 is the path length, and C_i is the concentration of component i in moles/liter (M). The application of Eq. (1) will provide an average concentration over the path of a beam that an be specified by the point it intersects the abscissa (r) of a coordinate system that is rotated at an angle (θ) from the laboratory frame of reference (Fig. 1). The relationship between these coordinates is given by the standard transformation in Eq. (2),

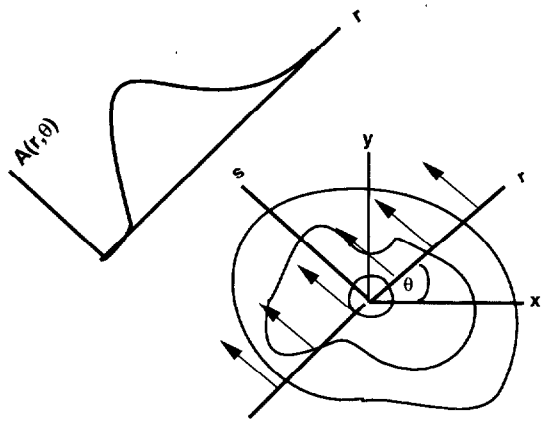

Fig. 1. The image of the property field can be reconstructed from a series of line-of-sight measurements taken as a function of r and θ.

$$\begin{aligned} x &= r\cos\theta - s\sin\theta \\ y &= r\sin\theta + s\cos\theta, \end{aligned} \tag{2}$$

where (x, y) and (r, s) specify the positions in the laboratory and rotated coordinate systems, respectively.

A map of the concentrations at every point in space can be constructed by the application of Eq. (1) to the corresponding local absorbance spectrum, $a_\nu(x, y)$, where the relationship between the local and line-of-sight spectra is expressed in Eq. (3),

$$A_\nu(r, \theta) = \int_0^l a_\nu(r, s)\, ds. \tag{3}$$

The inversion of Eq. (3) is achieved by application of the central slice [3] and convolution [17] theorems to give the local absorbance as the filtered back projection,

$$a_\nu(x, y) = \frac{1}{2\pi}\int d\theta \int [A_\nu(r, \theta)\phi((x\cos\theta + y\sin\theta) - r)]dr, \tag{4}$$

of the line-of-sight spectra. The filter function, ϕ, which arises from the Jacobian of the transformation from Cartesian into polar coordinates, can be parameterized to provide an optimal trade-off between spatial resolution and noise suppression. The set of $A_\nu(r, \theta_i)$ corresponding to a single-view angle is called a projection. Thus, Eqs. (1) and (4) provide a prescription for obtaining the concentrations of gases in a circular cross-section of the atmosphere from a series of projections measured as a function of the angle of view. The reconstruction of a three-dimensional volume can be obtained by stacking cross-sections.

The first step in assessing the feasibility of using computed tomography to evaluate the predictive capabilities of fire models is to determine the number of line-of-sight measurements required to obtain a desired level of accuracy in reconstructions of the component concentrations in a fire-generated plume. Questions of this nature are usually addressed by reference to the Nyquist theorem [18], which indicates that an image can be discretized without loss of information provided that it is sampled at a spatial frequency that is at least twice the value of its highest component frequency (Ω). The range of frequencies between 0 and Ω spans the space of the image and is called the bandwidth. The application of this theorem to the problem of interest, along with the assumption that the image has finite extent (i.e., $a_\nu(x, y) \to 0$ as $R = (x^2 + y^2)^{1/2} \to \infty$) results in the criterion expressed in Eq. (5),

$$N_\Theta = 2R\pi\Omega$$
$$N_r = 4R\Omega, \tag{5}$$

where N_θ is the number of projections and N_r is the number of line-of-sight measurements per projection.

This analysis, although meaningful when the purpose of the reconstruction is to resolve small defects in large irregular objects (which is almost always the case in medical and industrial applications of computed tomography), is misleading when it is applied to the problem of measuring concentrations in fire atmospheres because it does not account for the underlying structure of the plume. Indeed, in the absence of wind or physical obstructions to the flow, time-averaged plumes appear to exhibit a high degree of axisymmetry. This is advantageous because the projections of an axisymmetric image are the same from any view and only a single projection is needed to obtain a perfect reconstruction. Unfortunately, the instantaneous structure of a fire-generated plume is almost always distorted as a consequence of both external conditions and turbulence. The number of projections required for accurate reconstructions will naturally increase with the magnitude of the deviations from axisymmetry. Nevertheless, we will show that, in many cases of practical interest, these deviations are sufficiently small that it is possible to obtain an acceptable level of accuracy from reconstructions derived from a relatively small number of projections.

EXPERIMENTAL

Tomographic Measurements of Smoldering Wood Fires

The spatial distribution of component concentrations in the plumes above a series of small wood fires were obtained from spectroscopic measurements taken at z/r = 1, 1.5, 3, 4 and 5.5, where r and z denote the radius of the electric hotplate (0.09 m) that was used as the-heat source and thc axial distance from its surface, respectively. The fuel consisted of 186 g of American beechwood that was cut into blocks (10 mm × 20 mm × 35 mm) and placed uniformly in concentric circles on the surface of the hotplate [19]. The density of the wood, which had been stored in a conditioning room maintained at 28°C and 50% relative humidity prior to the experiments, was 760 kg/m^3. The hotplate achieved a maximum temperature of about 600°C that was usually reached about 10 minutes into the experiments. A high degree of repeatability of the centerline temperatures (Fig. 2a), velocities (Fig. 2b), and component concentrations was noted in a previous investigation of the properties of similar fires [20]. This provides the justification for the strategy used in this study, which consisted of splicing cross-sectional data measured in independent experiments to reconstruct a representative volume.

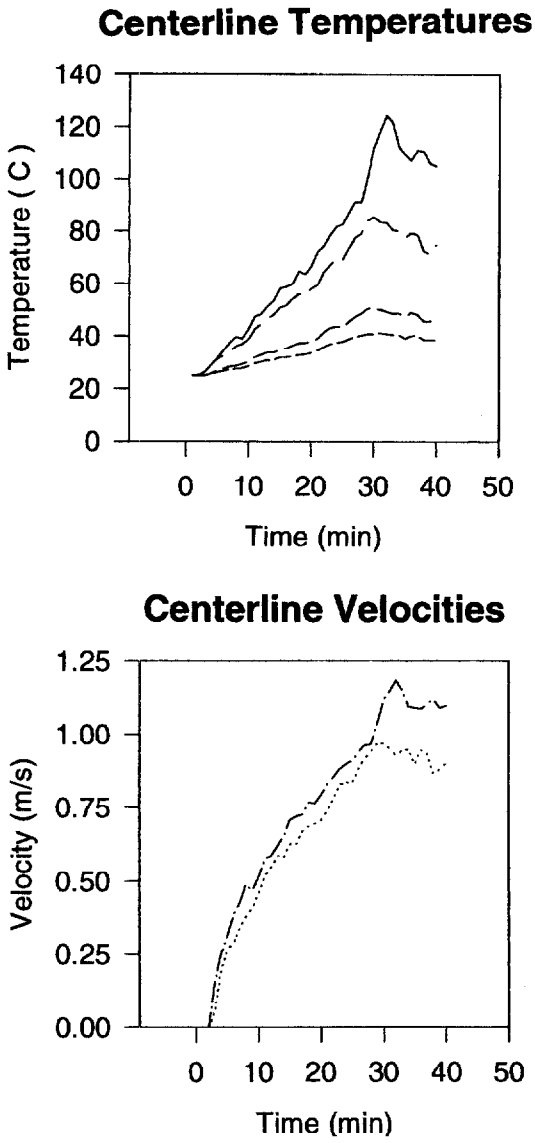

Fig. 2. The centerline temperatures (a) and velocities (b) measured at various heights in the plume above a smoldering wood fire.

The spectra were measured over the mid-infrared region extending from about 850 cm^{-1} to 4000 cm^{-1} at 4 cm^{-1} resolution using a Midac[1] open path Fourier transform infrared (FTIR) spectrometer. Each interferogram was signal averaged over 16 scans prior to performing the Fourier transformation.

[1] Certain commercial equipment, instruments, materials or companies are identified in this paper in order to specify adequately the experimental procedure. This in no way implies endorsement or recommendation by NIST.

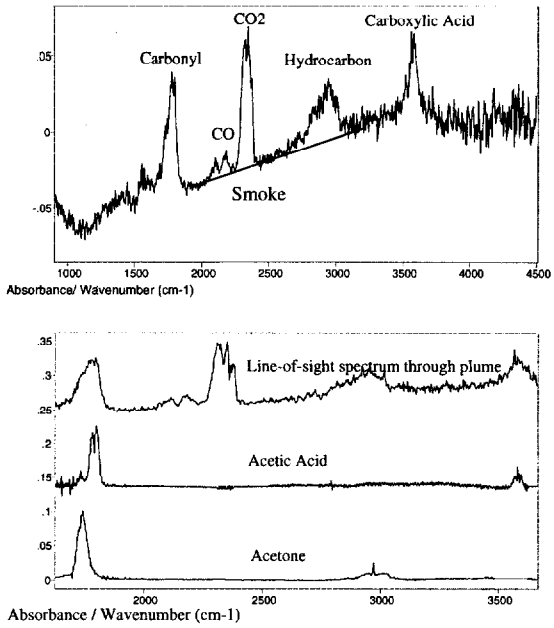

Fig. 3. A typical spectrum measured (at a resolution of 4 cm^{-1}) over a line-of-sight traversing the plume (a). The presence of particulates (smoke) is indicated by the sloping baseline. The assignments for CO (2045–2230 cm^{-1}) and CO_2 (2250–2400 cm^{-1}) are unambiguous. The assignment of the bands ranging from 1625 to 1760 cm^{-1}, and 3545 to 3625 cm^{-1} to acetone and acetic acid, respectively, were made on the basis of comparisons to reference spectra (b) that were acquired at a resolution of 0.5 cm^{-1}.

A typical spectrum measured over a line-of-sight traversing the plume is displayed in Fig. 3a. The assignments (Table 1) for CO (2045 cm^{-1}–2230 cm^{-1}) and CO_2 (2250 cm^{-1}–2400 cm^{-1}) are unambiguous. The absorption bands between 1625 cm^{-1} and 1760 cm^{-1}, and between 3545 cm^{-1} and 3625 cm^{-1} were tentatively assigned to acetone and acetic acid, respec-

TABLE 1

Characteristic Bands and Absorption Coefficients for Component Gases

Component	CO	CO_2	CH_3COOH	CH_3COCH_3
Frequency Range (cm^{-1})	2045–2230	2250–2400	3545–3625	1625–1760
Band Integrated Absorption Coefficients (M^{-1} m^{-1} cm^{-1})	182613	679538	159835	458073

tively. These assignments, which are consistent with characterizations made in previous investigations of smoldering wood fires [21–23], were based on the comparisons to reference spectra that are displayed in Fig. 3b. The peak between 3545 cm^{-1} and 3625 cm^{-1}, which overlaps with the band corresponding to the symmetric stretching mode in water at 3650 cm^{-1}, is characteristic of carboxylic acids. The interference with H_2O was negligible as long as the wood continued to smolder in the absence of flames, which was always the case when the spectra analyzed in this paper were measured. The broad band in the spectrum of the plume that ranges from about 1625 cm^{-1} to 1850 cm^{-1} can be accounted for by superimposing the carbonyl bands from the spectra of acetone and acetic acid.

The concentrations (C) of the target compounds were obtained from Eq. (6),

$$\frac{C_p}{C_c} = \frac{a_p l_c}{a_c l_p}, \tag{6}$$

where a_p is the integrated absorbance over a characteristic band of the target gas (Table 1), and 1 is the corresponding path length over which the absorption measurements were taken. The subscripts are used to distinguish between the measurements of the target gas in the plume above the fire (p) and in the calibration cell (c).

The calibration measurements for CO and CO_2 were made on Matheson reference gases in a 10 cm gas cell at 25°C. The calibrations for acetic acid and acetone were made on the basis of reference spectra in the Hanst quantitative library [24]. A minimum uncertainty of about 5–10% in the line-of-sight concentration measurements would be expected on the basis of past experiences with the quantitative analyses of similar compounds [20, 25–27]. This estimate, however, does not account for systematic errors arising from neglect of the temperature dependence of the absorption coefficients and deviations from Beer's law due to saturation of spectral lines. Although optical thickness would be expected to become an issue in larger fires, none of the characteristic peaks used in the quantitative analyses of the spectra measured in this study exhibited intensities exceeding 0.1 absorbance units. This is far below the empirical value of 0.7 absorbance units that is commonly used as the cutoff criterion for the application of Beer's law [28]. The error that results from the neglect of the temperature dependence of the absorption coefficients is more significant. However, a recent study of the temperature dependence of the infrared spectra of combustion gases, which was conducted in this laboratory, indicated that the integrated absorbance in CO_2 varies by less than 10% over the temperature range spanned in the plume (25–125°C). Furthermore, the centerline concentrations of CO and CO_2 obtained from analyses of line-of-sight FTIR spectra were shown to be in close agreement with the values obtained from NDIR measurements (of gas samples that were extracted from the plume and cooled to room temperature) in previous measurements made on smoldering wood fires [20].

The presence of particulates (smoke) is inferred from the sloping baseline in the line-of-sight spectra. The volume fraction (f_v) of smoke was obtained by fitting the empirical function, 1.50 f_v/λ, to the measured spectra over the region between 5 μm (2000 cm^{-1}) and 3.125 μm (3200 cm^{-1}). The range of applicability of this approximation is discussed in the classic text by Siegel and Howell [29] and references given therein.

The component concentrations in each cross-section were reconstructed as filtered back projections over 50 view angles using a modified Shepp-Logan filter in accord with Eq. (4) [4]. Only four projections (acquired at 45° increments between 0 and 180°), each consisting of 11 line-of-sight spectra scanned at 2.5 cm intervals (Fig. 1), were actually measured. These measurements were interpolated to provide the set of 550 spectra ($N_r = 11, N_\theta = 50$) that were used in the reconstructions. The effect of the interpolation was to produce smoother images than would have been obtained if we had only used the 44 ($N_r = 11, N_\theta = 4$) line-of-sight spectra that were actually measured in the filtered back projection calculations.

The optical design for tomographic scanning is displayed in Fig. 4. The acquisition of the 44 line-of-sight spectra used to reconstruct the component concentrations in each cross-section required about four minutes (i.e., one minute/projection). The time evolution of the plume

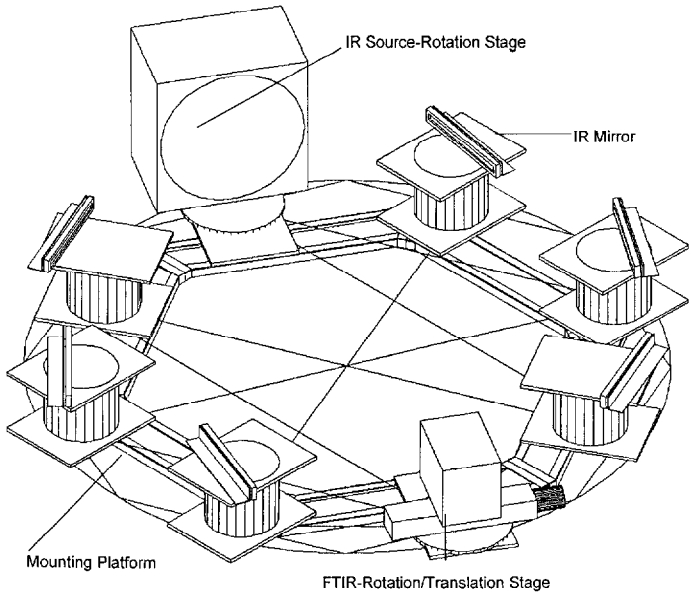

Fig. 4. Optical design of the multiangular tomographic spectrometer. The lines indicate the ray paths that which provide the four view angles.

was captured by making the measurements for each cross-section in a separate experiment. A total of 28 projections were acquired at each of the specified heights. This data was then regrouped into 25 frames, each consisting of projections at 0, 45, 90, and 135 degrees, which were constructed by successively replacing the oldest projection with the most recent set of measurements taken at the same angle (i.e., 1234, 5234, 5634, 5674, 5678, and so on, where the numbers indicate the order in which the projections were measured). In this way, a running average with a time resolution of approximately one minute was obtained. The optical platform was then translated to accommodate another height before repeating the process with a new fire.

Computer-Generated Plume

Computer simulations of the plume above a 0.25 m gas burner with a heat release rate of approximately 35 kw were performed using the NIST Large Eddy Simulation Model [30–32]. In this model, the mixing and transport of combustion products are calculated directly from an approximate form of the Navier-Stokes equations. The equations were solved over a $1 \times 1 \times 2$ m^3 volume using a rectangular grid consisting of 64^3 elements with a time step of 0.01 s. The criteria used to determine the spatial and temporal resolution of the calculations are discussed in detail elsewhere [32].

An analysis to determine the number of line-of-sight measurements needed to represent the turbulent structure of fire-generated plumes was made by performing reconstructions of the time-dependent mixture fraction field (X) as functions of N_r and N_θ in a 0.12 m^3 segment of the plume (represented by 25^3 volume elements) centered approximately 1 m above the burner. The mixture fraction is a conserved scalar quantity that is defined as the fraction of the total mass in the plume originating from the fire source. Consequently, it provides an unambiguous measure of the degree of mixing at any position in the plume. In principle, there is a direct proportionality between the mixture fraction field and the experimentally determined component concentrations. More specifically,

$$C_i(x, y, z) = \rho \epsilon_i X(x, y, z), \tag{7}$$

where ρ is the density (mass/volume) of the plume and ϵ_i is the yield of component i (moles) per unit mass of fuel burned.

The time-dependent mixture fraction field was represented by 25 cross-sections that were updated every 0.01 s for 100 time steps. The ($N_r \times N_\theta$) line-of-sight measurements correspond-

ing to each cross-section were evaluated by numerical integration [33] of the computer-generated mixture fraction field along 500 uniformly spaced rays at each of N_θ view angles. The number of radial measurements was reduced from 500 to N_r by averaging each line-of-sight over $500/N_r$ values. This simulates the measurement process with a square aperture of width 40 cm/N_r and ensures conservation of mass by completely irradiating the sample.

RESULTS AND DISCUSSION

Tomographic Measurements of Smoldering Wood Fires

A composite image of the plume constructed by stacking five cross-sectional slices of the concentration (in units of moles/liter) of CO is displayed in Fig. 5. The spatial variation within the volume is indicated by iso-surfaces (differentiated by shades of grey) that connect regions that have the same concentration. The data for each time dependent cross-section, consisting of 44 line-of-sight spectra, were measured in independent fires over a four-minute interval approximately halfway through the burn. The qualitative features, including the approximate axisymmetry and expansion of the plume as a function of vertical distance from the fire source, are apparent. The temporal resolution of these measurements is obviously far too coarse to provide detailed information about the turbulent fluctuations in the component concentrations. Nevertheless, the spatial dependence of the time-averaged concentrations is revealing and provides an experimental reference point for the analysis of the more highly time-resolved data obtained from the computer-generated plume.

A closer examination of the individual cross-sections reveals additional insights into the structure of the plume. A representative plot showing the spatial distribution of CH_3COOH in a cross-sectional volume 1 radius above the hotplate is displayed in Fig. 6. The results obtained from least squares fits [34] of the concentrations of CO, CO_2, CH_3COCH_3, CH_3COOH and smoke to the 4 parameter normalized Gaussian function in Eq. (8)

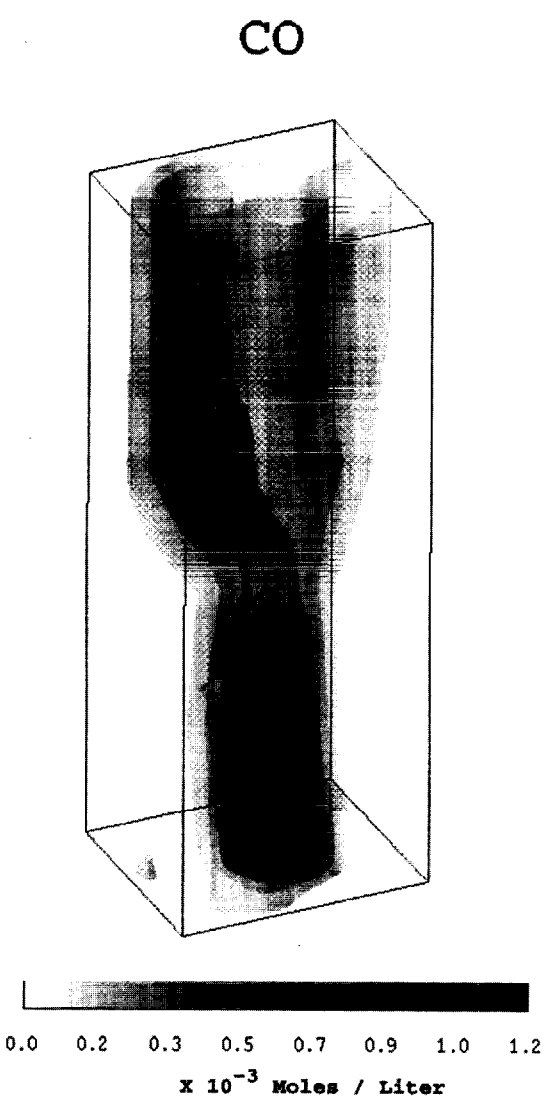

Fig. 5. Volume reconstruction of the concentrations (M) of CO in the plume above a smoldering wood fire.

$$G_i(x, y) = \left(\frac{c_i a_i}{\pi}\right) \exp\left(-a_i((x - b_{ix})^2 + (y - b_{iy})^2)\right) \quad (8)$$

are summarized in Table 2. The high degree of accuracy provided by the Gaussian fits is consistent with the analysis presented by Shabbir and George [35].

The physical interpretation of the parameters that comprise the Gaussian model of the plume is straightforward. Thus, the position of the peak concentration (the coordinates range from

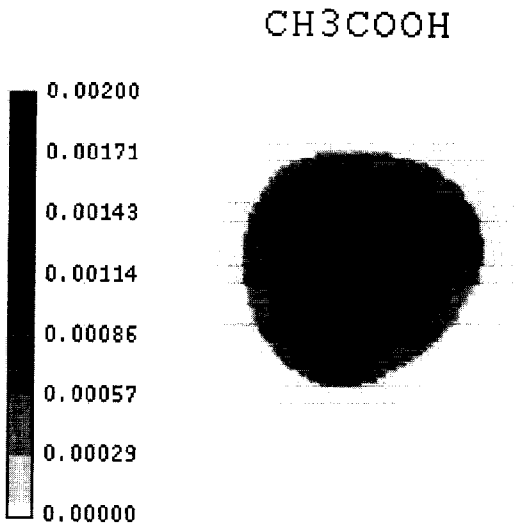

Fig. 6. Contours of the concentrations of CH_3COOH (M) at $z/r = 1$ approximately halfway through the burn.

0 to 24) is defined by the parameters (b_x,b_y), and a is inversely proportional to the (square root of the) width of the plume. The value of c_i is proportional to the mass of component i (Eq. [11]) that occupies a cylindrical volume of the plume defined by the radius of the scan (12.5 cm) and the width of the infrared beam (~2 cm). In principle, c_i should be a constant independent of height as long as there are no reactions in the plume. In fact, there are significant fluctuations in the observed data (Table 2) that we attribute to random error introduced in the process of employing cross-sectional measurements obtained from a series of fires in the construction of the composite image of the plume.

The data listed in Table 2 indicate that the concentrations of the gases in each cross-section are reasonably well-described by a single Gaussian function that increases in width with increasing values of z/r as expected. The Gaussian that describes the smoke, however, appears to be broader, at least in the region close to the smoldering wood. The source of this disparity is not clear, but it may be a consequence of the temperature gradient across the hotplate. These data also appear to indicate that there is a reaction in the plume that leads to the formation of a ketone at the expense of carboxylic acid. This effect is much more evident in computer movies of the time-dependent concentrations that clearly show a pronounced decrease in the concentration of CH_3COOH and a corresponding increase in the concentration of CH_3COCH_3 at a height of about $z/r = 3$. This observation is consistent with the possibility that there is a bimolecular condensation reaction, such as the one depicted in Eq. (9),

TABLE 2

Gaussian Fits of the Component Concentrations

Height (z/r)	Parameters/Standard Error	CO	CO_2	RCOOH	RCOR	Smoke
1	c_i	0.074	0.074	0.22	0.078	2.7×10^{-5}
	a_i	0.03	0.03	0.04	0.04	0.02
	b_{ix}, bi_y	13, 14	13, 15	13, 14	13, 14	13, 14
	SE	4×10^{-5}	8×10^{-5}	1×10^{-4}	5×10^{-5}	4×10^{-10}
1.5	c_i	0.065	0.094	0.20	0.049	2.4×10^{-5}
	a_i	0.03	0.03	0.03	0.04	0.02
	b_{ix}, b_{iy}	13, 13	13, 15	13, 13	13, 14	13, 15
	SE	4×10^{-5}	5×10^{-5}	1×10^{-4}	2×10^{-5}	4×10^{-10}
3	c_i	0.033	0.078	0.069	0.11	3.9×10^{-5}
	a_i	0.03	0.03	0.04	0.02	0.02
	b_{ix}, b_{iy}	13, 14	13, 12	12, 13	13, 12	13, 13
	SE	2×10^{-5}	8×10^{-5}	5×10^{-5}	4×10^{-5}	6×10^{-10}
4	c_i	0.094	0.078	0.16	0.12	4.9×10^{-5}
	a_i	0.01	0.01	0.01	0.01	0.01
	b_{ix}, b_{iy}	12, 11	12, 13	12, 11	12, 12	12, 11
	SE	5×10^{-5}	4×10^{-5}	7×10^{-5}	4×10^{-5}	7×10^{-10}
5.5	c_i	0.082	0.11	0.094	0.12	5.0×10^{-5}
	a_i	0.01	0.01	0.01	0.01	0.01
	b_{ix}, b_{iy}	11, 13	12, 12	12, 12	13, 10	13, 12

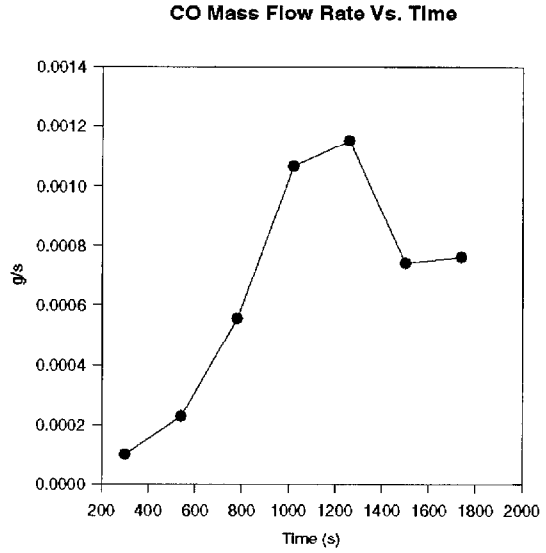

Fig. 7. The mass output of CO from the smoldering wood fire as a function of time.

$$2CH_3COOH \Rightarrow CH_3COCH_3 + CO_2 + H_2O, \quad (9)$$

occurring in the plume. This explanation seems more plausible than the alternative of unimolecular decomposition that would not explain the observed increase in CH_3COCH_3 and that would not be expected to occur at the low temperatures (~100°C) and relatively high concentrations of CH_3COOH (~5%) that prevail in the plume.

The standard errors (SE) of the fits were computed in accord with Eq. (10),

$$SE = \left[\frac{\int (C_i(x,y) - G_i(x,y))^2 dxdy}{N(N-1)} \right]^{1/2}, \quad (10)$$

where $C_i(x,y)$ is the reconstructed concentration of component i at the point (x,y). The SE values are on the order of 10^{-4} or less (compared to the peak concentrations that are on the order of 10^{-2}), which suggests that an accurate representation of the time-averaged component concentrations could have been obtained by fitting a Gaussian function at each cross-section. In principle, this means that the number of line-of-sight measurements/cross-section could have been reduced from 44 to 4 with only a small sacrifice in accuracy.

The emissions from wood fires are sometimes expressed in terms of the ratio of the component concentrations to that of CO [21] because CO is both convenient to measure and symptomatic of the combustion process. The mass flow of CO, which is represented in Fig. 7, was obtained from Eq. (11),

$$m(t) = Mc(t)v(t)\Delta A, \quad (11)$$

where $c(t)$ is the parameter from the Gaussian fit (at $z/r = 1$) to the CO concentrations at time t (Table 3), $\Delta A = \Delta x \Delta y = 1.62 \times 10^{-4}$ m^2 is the area corresponding to the volume elements used in the numerical integration of this function, and $M = 28$ g/mol is the molecular weight of CO. The time-dependent velocity ($v(t)$) was obtained from centerline measurements at $z/r = 2$ (Fig. 2).

Computer-Generated Plume

The convergence of the reconstructions of the instantaneous mixture fraction field as a function of N_r and N_θ is summarized in Fig. 8. The error was computed by averaging the absolute values of the differences between the actual and reconstructed mixture fraction fields (normalized by dividing by the actual value) over a set of 625 cross-sections corresponding to 25 vertical positions at 100 time steps. On this basis, it appears that it requires a minimum of about 275 line-of-sight measurements/cross-section (N_r =

TABLE 3

Parameters for the Time-Dependent Gaussian Representation of the Plume at $z/r = 1$

Time (s)/Parameter	0	240	480	720	960	1200	1440
c_i	0.016	0.024	0.045	0.073	0.069	0.047	0.036
a_i	0.01	0.02	0.03	0.03	0.03	0.02	0.01
b_{ix}	13	14	13	13	13	14	14
b_{iy}	2	15	14	14	14	12	10
SE	2.4×10^{-5}	2.4×10^{-5}	2.4×10^{-5}	2.4×10^{-5}	2.4×10^{-5}	2.4×10^{-5}	

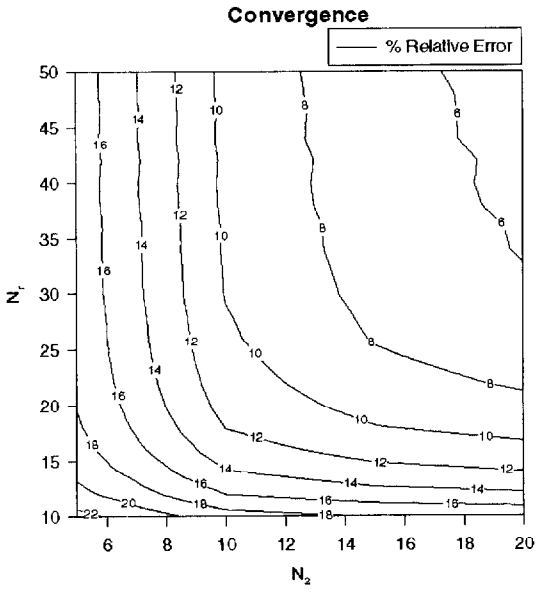

Fig. 8. The convergence of the reconstructions of the instantaneous mixture fraction field as a function of N_r and N_θ. The error was computed by averaging the absolute values of the differences between the actual and reconstructed mixture fraction fields (normalized by dividing by the actual value and multiplying by 100 to convert into a percentage) over a set of 625 cross-sections corresponding to 25 vertical positions at 100 time steps.

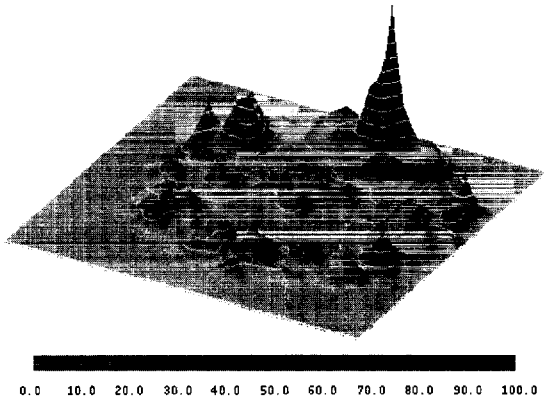

Fig. 9. The spatial distribution of the error in reconstructing a representative cross-section from 260 line-of-sight measurements (N_r = 26, N_θ = 10).

25, N_θ = 11) to reconstruct the time-dependent mixture fraction field of this plume with an average relative error of about 10%, which is comparable to the anticipated experimental error in the line-of-sight concentration measurements. The spatial distribution of the error in reconstructing a representative cross-section from 260 line-of-sight measurements (N_r = 26, N_θ = 10) is displayed in Fig. 9.

The f = 0.12, 0.4, and 0.6 iso-surfaces obtained from the actual mixture fraction field and a reconstruction obtained from 260 line-of-sight measurements (N_r = 26, N_θ = 10) per cross-section at t = 0.5 s (halfway through the simulation) are compared in Fig. 10. The close agreement is surprising since the model calculations were resolved over a much finer grid (25^2 = 625 volume elements). Indeed, the bandwidth (Ω_r) of the mixture fraction field, as indicated by the dominant peak in the power spectrum of the Fourier transformation [36] (with respect to r) of representative projections, is about 0.25 measurements/cm (Fig. 11). Substitution of this value into Eq. (5) gives N_r = 20 and N_θ = 30, which implies that about 600 line-of-sight measurements (i.e., approximately one measurement for each volume element) should be required to recover the image without loss of information. This result, however, does not reflect the reduction in measurement requirements due to the underlying axisymmetry of the plume. In fact, the Fourier transform of representative projections (at a constant value of r) with respect to θ (Fig. 12) indicate that the angular bandwidth is actually only about $4/\pi$ (measurements/rad). This implies that it only requires eight view angles to reconstruct the infinitesimal radial shell subjected to the angular frequency analysis. This is reasonably consistent with the results of the numerical experiments, which were conducted on the full volume of the plume, summarized in Fig. 8.

In the absence of wind or physical obstructions to the flow, the deviations in the structure of the plume from axisymmetry are due to turbulence. This suggests that the time dependence of the plume can be conceptualized by decomposing it into a steady-state axisymmetric component, which can be reconstructed from a single projection, and a fluctuating asymmetric component that requires many view angles to reconstruct but which averages to zero over time. The progression in the structure of the computer-generated plume (represented by the mixture fraction iso-surface f = 0.27), as a function of the length of time over which the mixture fraction field was averaged, is illustrated in Fig. 13. The underlying axisymmetry of

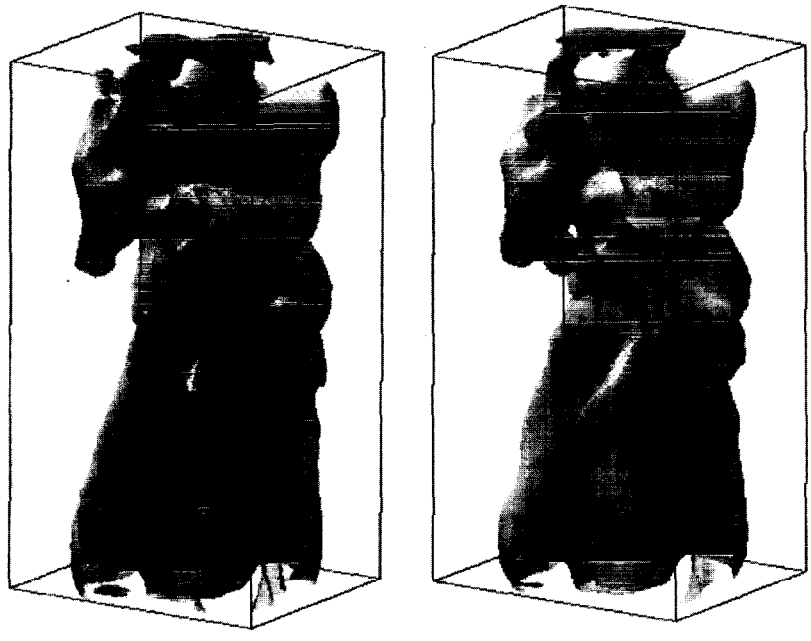

Fig. 10. Comparison of the f = 0.1, 0.4 and 0.6 iso-surfaces obtained from the complete mixture fraction data set and the reconstruction using 260 line-of-sight measurements/ cross-section.

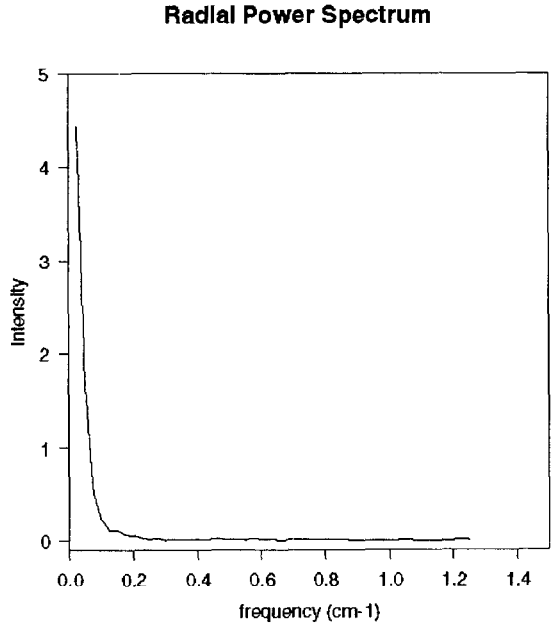

Fig. 11. Fourier transform with respect to r of a representative projection of the computer simulated mixture fraction field. The bandwidth, as indicated by the extent of the dominant peak, is approximately one measurement for every 4 cm.

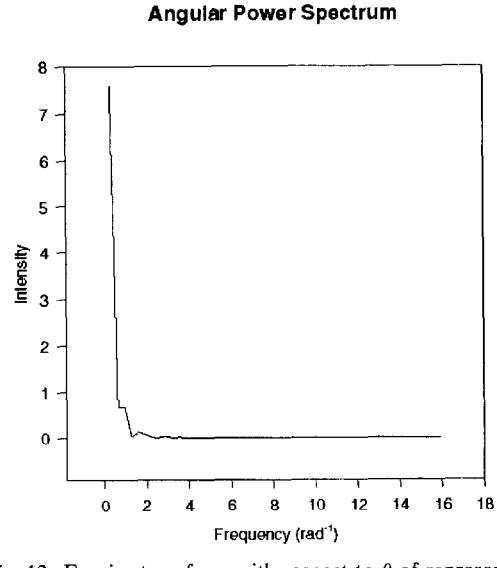

Fig. 12. Fourier transform with respect to θ of representative projections (at a constant value of r) of the computer simulated mixture fraction field. The bandwidth, as indicated by the extent of the dominant peak, is approximately four measurements per radian.

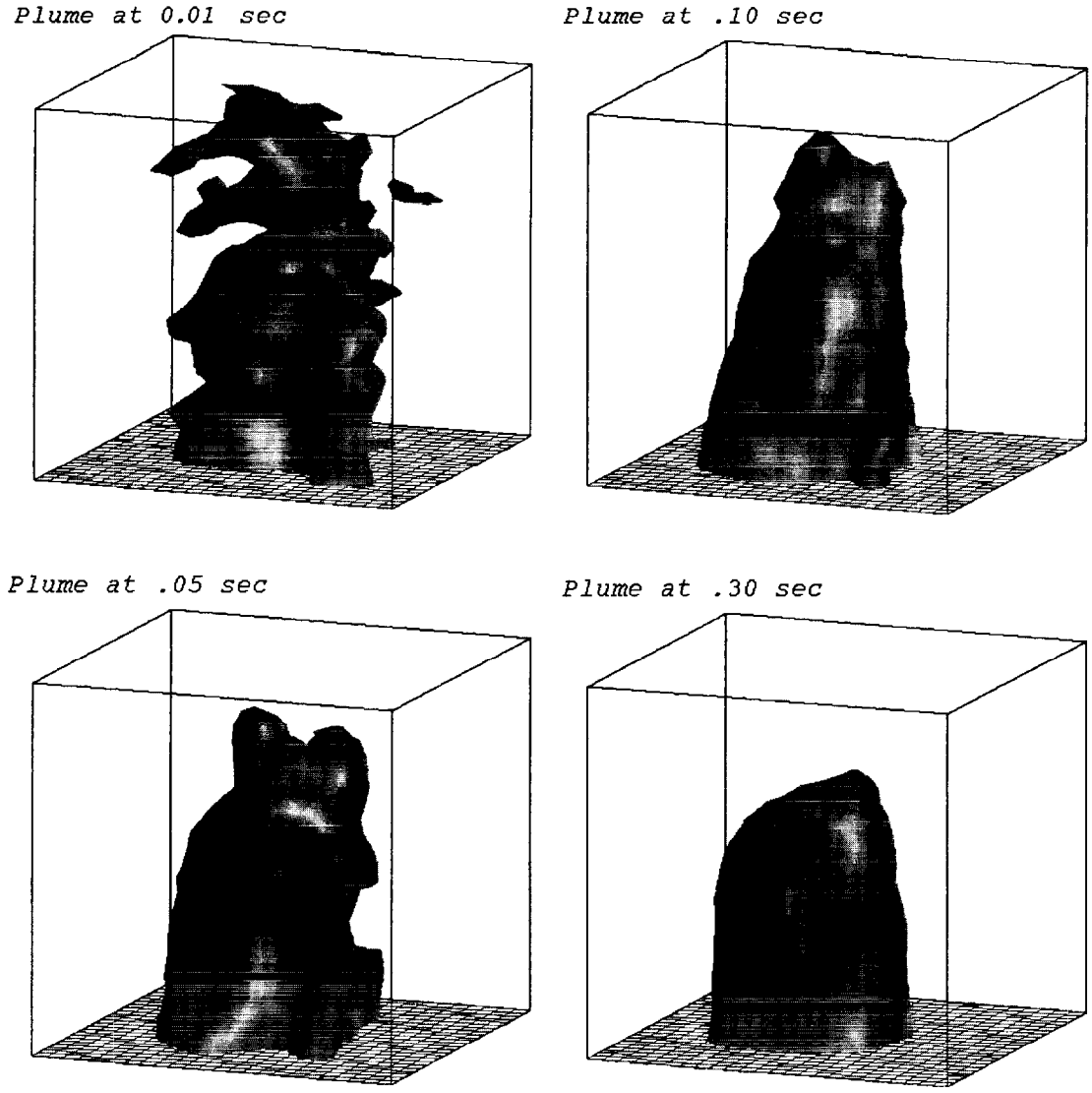

Fig. 13. The progression in the structure of the plume, as indicated by the $f = 0.27$ iso-surface, as a function of the length of time over which the mixture fraction field was averaged. The underlying axisymmetry of the plume is apparent at a time resolution of 0.3 s.

the plume begins to emerge at a time resolution of about 0.3 s. Presumably, this process continues until it converges to produce a cylindrical plume in the limit as $t \to \infty$. This is consistent with experimental observations that indicated that the contours of the component concentrations above the smoldering wood fires were nearly circular at a time resolution of about one minute.

The conceptualization presented above suggests that the magnitude of the errors in reconstructing the time-dependent mixture fraction field will depend on the relative contributions of the axisymmetric and asymmetric components. More specifically, the rate of convergence with respect to the number of view angles should decrease with increasing turbulent intensity of the flow field. However, since errors due to insufficient angular sampling of the asymmetric component will tend to integrate to zero over time, the statistics derived from a series of reconstructions may be accurate even if the

instantaneous mixture fraction field is not. The validity of this hypothesis is supported by Fig. 14 that compares a reconstruction of the instantaneous mixture fraction field ($N_r = 70$, $N_\theta = 4$) in the 12th cross-section (at $t = 0.5$ s), as well as the mean and variance derived from reconstructions of 100 time steps, to the corresponding quantities obtained from the model calculations. The increased accuracy of the time statistics (over what was obtained for the reconstruction of the instantaneous mixture fraction field), as indicated by the favorable agreement between the first two moments of the reconstructed and computer-generated mixture fraction fields [37], is beneficial since a comparison of the pdfs would be expected to be more revealing than a frame-by-frame comparison of the experimental and predicted property fields. This is a consequence of the chaotic nature of turbulence that implies that the instantaneous property field is not reproducible.

SUMMARY AND CONCLUSIONS

Analyses of tomographic measurements of component concentrations in the plumes above small smoldering wood fires at a time resolution of about one minute indicate that the spatial variation of these quantities are well described by a four-parameter Gaussian model. In principle, this means that as few as four line-of-sight measurements are sufficient for accurate reconstructions of the time-averaged component concentrations in a cross-sectional volume of the plume. This coarse temporal resolution, however, is not adequate to provide information about the turbulent fluctuations in the component concentrations. The analyses of computer-generated mixture fraction fields presented in this paper confirms the intuitive notion that the spatial density of measurements needed to obtain accurate reconstructions of turbulent plumes increases with the temporal resolution of the measurements. Nevertheless, the number of measurements needed to obtain an acceptable level of accuracy (on the order of 10% relative error), even in highly time resolved measurements ($\Delta t = 0.01$ s), is considerably less than what is conventionally used in typical applications of computed tomography.

The reduction (with respect to other applications of CT) in the density of measurements needed to characterize the spatial dependence of the flow field, which is a consequence of the underlying axisymmetry of the plume, can be exploited to increase the temporal resolution, quantitative accuracy, and the physical dimensions of the measurement space. On the basis of our analysis, the substitution of ten detector modules, arranged in a semicircle at intervals of 18° (each consisting of multiple elements spaced approximately 1.6 cm apart), for the translation stage and rotation platforms used in the current design would provide accurate time statistics while reducing the measurement time to about 15 Hz per cross-section which is the scan time of the interferometer. This increase in temporal resolution would be sufficient to resolve the pulsation frequencies in fires larger than about 10 cm in diameter. An additional order of magnitude reduction in acquisition time, however, would still be needed to capture the turbulent structure of fire-generated plumes in sufficient detail to provide for rigorous validations of CFD fire models such as the NIST Large Eddy Simulation Model. This goal is attainable provided that band pass filters or laser sources, rather than an FTIR spectrometer, are used to resolve compound specific spectral features.

A facility like the one described in the preceding paragraph could be constructed using commercially available components. The range of applicability, however, would be limited to measurements above small fires like the one considered in the present investigation, where the plume is optically thin and relatively cold. Nevertheless, such a facility would provide a much needed test bed that would enable investigators to calibrate and validate their models in the laboratory before applying them to full-scale fires.

We are grateful to Professor William Davis (Montgomery Community College) for his help in the design and construction of the tomographic spectrometer, to Dr. Pumyos Vallikul (King Mongkut's Institute of Technology) for assistance in writing the reconstruction software, and Dr. Howard Baum (NIST) for his encouragement and helpful discussions.

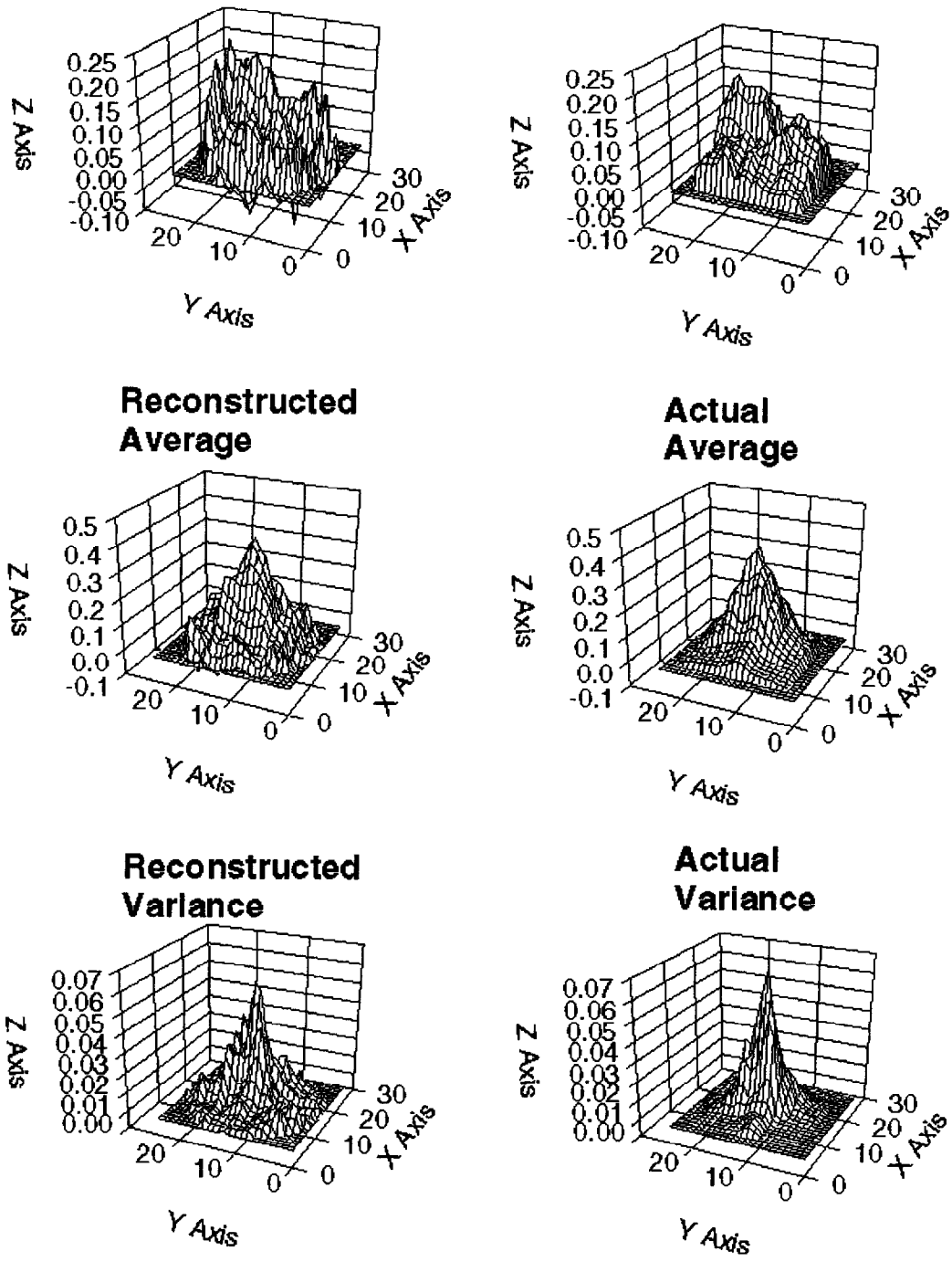

Fig. 14. The spatial distributions of the mean and variance derived from reconstructions ($N_r = 70$, $N_\theta = 4$) of 100 frames of the instantaneous mixture fraction field in the 12th cross-section (approximately halfway up the plume) are compared with the corresponding quantities computed directly from the results of the model calculations. The comparison between a reconstruction of the instantaneous mixture fraction field and the model calculations (at $t = 0.5$ s) is less favorable.

REFERENCES

1. Fisher, S. J., and Grosshandler, W. L., *Twenty-Second Symposium (Int'l) on Combustion:* 1241 (1986).
2. Bouhafid, A., Vantelon, J. P., Joulain, P., and Fernandez-Pello, A. C., *Twenty-Second Symposium (Int'l) on Combustion:* The Combustion Institute, University of Washington, Seattle, Washington 1291 (1986).
3. Azevedo, S. G., *Model-based Computed Tomography for Nondestructive Evaluation,* University of California, Livermore, 1991.
4. Shepp, L. A., and Logan, B. F., *IEEE Trans. Nucl. Sci.* **NS-21**:21 (1974).
5. Ramachandran, G. N., and Lakshminarayanan, A. V., *Proc. Natl. Acad. Sci. U.S.* 68:2236 (1971).
6. Emmerman, P. J., Goulard, R., Santoro, R. J., and Semerjian, H. G., *J. Energy* 4:70 (1980).
7. Santoro, R. J., Semerjian, H. G., Emmerman, P. J., and Goulard, R., *Int. J. Heat Mass Transfer* 24:1139 (1981)
8. Best, P. E., Chien, P. L., Carangelo, R. M., and Solomon, P. R., *Combust. Flame* 85:309 (1991).
9. Bates, S. C., Carangelo, R. M., Knight, K., and Serio, M., *Rev. Sci. Instrum* 64:1213 (1993).
10. Budinger, T. F., and Gullberg, G. T., *IEEE Trans. Nucl. Sci.* NS-21:2 (1974).
11. Cho, Z. H., *IEEE Trans. Nucl. Sci.* NS-21:44 (1974).
12. Swindell, W., and Barrett, H. H., *Physics Today* December: 32 (1977).
13. Sivathanu, Y. R., and Gore, J. P., *JQSRT* 49:269 (1993).
14. Nyden, M. R., Vallikul, P., and Sivathanu, Y. R., *JQSRT* 55, (3):345 (1996).
15. Lee, K-O. and Choi, M. Y., Thirtieth Section Anniversary Tech. Meeting, Central States Section, The Combustion Institute: 146, 1996.
16. Greenberg, P. S., and Ku, J. C., *Combust. Flame* 108:227 (1997).
17. Arfken, G., *Mathematical Methods for Physicists,* Academic Press, New York, 1970, p. 681.
18. Oppenheim, A. V., and Schafer, R. W., *Digital Signal Processing,* Prentice-Hall, Englewood Cliffs, NJ, 1975.
19. Comité Européen de Normalization (C.E.N.) 54: Components of Automatic Fire Detection Systems; Part 9, Fire sensitivity test. European Committee for Standardization, 1982.
20. Cleary, T., Grosshandler, W., Nyden, M. R., and Rinkinen, W., *Proceedings of the Seventh International Interflam Conference,* (C. A. Franks and S. Grayson, Eds.), Interscience Communications Ltd., London, 1996, pp. 235–243.
21. McKenzie, L. M., Hao, W. M., Richards, G. N., and Ward, D. E., *Atm. Environ.* 28(20):3285 (1994).
22. McKenzie, L. M., Hao, W. M., Richards, G. N., and Ward, D. E., *Environ. Sci. Technol.* 29:2047 (1995).
23. Degroot, W. F., Pan, W-P., Rahman, M. D., and Richards, G. N., *J. Analyt. Appl. Pyrol.* 13:221 (1988).
24. Hanst, P. L., and Hanst, S. T., *Quantitative Reference Spectra for Gas Analysis* (1990), Infrared Analysis, Inc., Anaheim.
25. Nyden, M. R. Grosshandler, W., Lowe, D. L., Harris, R., and Braun, E., *NISTIR* 5280:65 (1993).
26. Nyden, M. R., Grosshandler, W., Lowe, D. L., Harris, R., and Braun, E., *Optical Sensing For Environmental Monitoring* SP-89:767 (1993).
27. Nyden, M. R., and Babrauskas, V. Twentieth Fall Technical Meeting of the Eastern Section, The Combustion Institute, 107 (1987).
28. Griffiths, P. R., and deHaseth, J. A., *Fourier Transform Infrared Spectrometry,* John Wiley & Sons, New York, 1986, p. 339.
29. Siegel, R., and Howell, J. R., Thermal Radiation Heat Transfer, 3rd ed., Hemisphere, Washington, DC, 1992, p. 660.
30. Rehm, R. G., and Baum, H. R., *J. Res. of the NBS* 83:297 (1978).
31. McGrattan, K. B., Baum, H. R., and Rehm, R. G., *J. Comp. Phys.* 110(2):285 (1994).
32. Baum, H. R., McGrattan, K. B., and Rehm, R. G., *J. Heat Transfer Soc. Japan* 35(139):45 (1996).
33. Press, W. H., Flannery, B. P, Teukolsky, S. A., and Vetterling, W. T., *Numerical Recipes in C, Cambridge University Press,* Cambridge, UK., 1988, p. 120.
34. *Sigmaplot,* Jandel Corp., San Rafael, 1994.
35. Shabbir, A., and George, W. K. NASA Technical Memorandum 105:955 (1992).
36. Wolfram, S., *Mathematica,* 2nd ed., Addison-Wesley, Redwood City, 1991, p. 679.
37. Mood, A. M., Graybill, F. A., and Boes, D. C., *Introduction to the Theory of Statistics,* McGraw-Hill Book Company, New York, 1974, p. 150.

Received 20 November 1996; accepted 20 June 1997